HEAT TRANSFER IN POST BURST ACCIDENT MODELS

T.J. MARCINIAK,

Reactor Analysis and Safety Division, Argonne National Laboratory, Argonne, Illinois, U.S.A.

ABSTRACT

Continuation of post-burst accident analyses in Liquid Metal Fast Breeder Reactors (LMFBR) from the initial shock phase and into the blast phase necessitates the consideration of heat transfer effects; especially those which have an ameliorating effect upon the destructive work potential of the energy deposited in the core materials. In general, programs to handle conduction, convection and radiative heat transfer in large, post-burst analysis codes such as REXCO-H would be too unwieldy and would still necessitate specialized models to accommodate intracell heat transfer models such as molten fuel-coolant interactions. The paper describes the general classification of heat transfer models on both intra- and intercell basis for use in the REXCO-H hydrodynamics code. Following this general discussion is a detailed account of the incorporation of an intercell conduction model and an intracell fuel-coolant interaction model. Preliminary results from these two models are also included.

1. INTRODUCTION

In order to treat the analysis of postulated liquid metal fast breeder reactor (LMFBR) accidents for longer times as well as to realistically evaluate their effects on the primary containment, improved energy partition estimates including heat transfer must be made. The area of heat transfer effects in post burst accident analysis programs is quite undefined since the dominant modes of heat transfer are heavily dependent upon the configuration, or state, of the reactor at the termination of the nuclear excursion, or burst.

For instance, in the case of an extremely energetic accident, the state of the reactor may be such that the core region has been completely vaporized. Here the dominant mode of heat transfer might well be radiation with convection. However, it is also possible to postulate a less energetic accident in which the fuel has melted but the sodium coolant is still present, either due to reentry or fuel meltdown occurring before sodium expulsion. In this case the dominant mode of heat transfer would involve conduction, convection and boiling in a molten fuel-coolant interaction. Aside from the dominant modes of heat transfer enumerated above, the results of heat transfer cause in the first case a reduction of pressure due to energy transfer from a hot to cold zone, while in the second case a pressure source for damage propagation due to a vapor explosion exists. Thus, in general, heat transfer effects can either help in the reduction of accident consequences or cause significant increase depending upon the rate and conditions of the heat transfer.

An unfortunate problem which is encountered, however, in accident analysis codes is that due to their basic complexity and size, there is little room left in high speed memory storage to be able to incorporate a generalized heat transfer code which would offer conduction, convection and radiation as options on an inter- and intracell basis. The basic difficulty, especially when one solves a set of hydrodynamic equations for large arrays in Lagrangian coordinates, is one of compatibility with the numerical technique. For instance, in the REXCO-H [1] hydrodynamic response program a numerical technique compatible with the mid-point method of differencing is desirable.

2. ENERGY DISSIPATION MECHANISMS

Of primary interest to reactor safety analysts is the defining of models which have a tendency to reduce the work potential of nuclear reactor energy bursts. This is especially the case in the fast reactor field where relatively small cores are operating at extremely high power densities with high coolant flow rates of the order of 9.0 m/sec. It is possible that in the event of an accident such as flow coastdown that a significant amount of energy may be added to the fuel before corrective action can be taken to either reduce reactor power or shut down. Even with quick corrective response one still must contend with the effects of fission product decay heat which must be removed to prevent reactor core damage.

Historically, estimates of the destructive potential of postulated nuclear excursions have been quite conservative. This was done under the valid supposition that if one demonstrates that a particular configuration can survive an accident whose work potential has been overestimated then, of couse, it should survive lesser, more probable, work potentials. One difficulty with this approach, however, is that in the case of the LMFBR it is possible to postulate a set of circumstances, which are thought to have extremely low, but not zero, probabilities of occurrence, in which the conservatively estimated destructive work potential cannot be absorbed and still assure the survival of the system. So it is imperative that better estimation of energy partitioning be made if one is to design an economical fast reactor.

Energy partitioning, then, enables one to answer the following question: Given a nuclear accident in a reactor with a given amount of energy, how much energy is in a) the core; b) the shock wave; c) kinetic energy; d) strain energy of the vessel and other components; and e) heat energy in the components. The strain energy in the vessel is the important quantity because if one knows its value one can then have some knowledge about how it would survive a postulated accident. The partitioning of energy is being carried out with a hydrodynamic code, REXCO-H and it deals with items a), b), c) and d) above. Item e) is taken care of somewhat in the code by changes in the specific internal energy of a given material, but mainly heat transfer considerations on an inter- or intracell basis must be made to completely consider this phenomena.

Heat transfer as a dissipative mechanism in post burst accident analyses occurs continuously in the shock wave where a high pressure, high temperature, narrow zone exists. This is normally taken care of by a heat conduction term. Energy dissipation by this method is relatively small compared to the initial shock wave energy. If one assumes that in an essentially instantaneous explosion about one-half of this energy is carried away in the shock wave, only a small fraction can be expected to be deposited in the medium through which the shock wave passed.

Still other means of dissipative heat transfer modes may be delineated especially in the region of the reactor core. This region can be considered to be quite hot and in some instances may even be composed of vaporized fuel and coolant at temperatures approaching 5000°K. Of course, less energetic accidents may not have such a high energy density and may consist of partially, or fully, melted fuel with or without sodium present. In either case, the core region is surrounded by a large mass of relatively cold materials consisting mainly of sodium and stainless steel structural materials. Heat transfer to this mass could have a strong effect on ameliorating the consequences of an accident not so much in the early stages of the post burst phase, of the order of tens of milliseconds, but at longer times. Its strongest effect may come when one considers the impingement of the sodium slug upon the reactor vessel head. Heat transfer to the surroundings may well cause rapid condensation of the core vapor bubble thus reducing its pressure and, of course, the loading in the sodium slug above the core.

3. ENERGY SOURCE MECHANISMS

Another consideration for heat transfer effects in post burst accident analyses is that of pressure sources. An example of this kind of phenomenon would be that encountered with the molten fuel-coolant interaction. If one postulates a volume in which molten fuel is present with sodium liquid, rapid heat transfer to the coolant can cause a violent vapor explosion. The highest pressures, however, occur during the liquid heating phase.

Pressure sources may also exist in those areas where rapid conductive or convective heat transfer from a hot region to an adjacent cold region as may occur between an extremely hot, high temperature, vaporized fuel zone and perhaps relatively cold sodium. In this case, rapid vaporization of sodium at the boundary could well cause higher long term system pressures.

4. CONDUCTION HEAT TRANSFER MODEL

As a first step in the incorporation of dissipative heat transfer mechanisms in REXCO-H, a conduction heat transfer term was added to the energy equation, i.e.

$$dE = -pdv + \frac{k}{\rho} \nabla^2 T \tag{1}$$

where E is the specific internal energy, p is the pressure, v is the specific volume, k is the thermal conductivity, ρ is the density, and T is the temperature. Since the REXCO-H code is an axisymmetric code, the second term on the right side of Eq. (1) is written

$$\frac{k}{\rho} \nabla^2 T = \frac{k}{\rho}\left(\frac{\partial^2 T}{\partial r^2} + \frac{1}{r}\frac{\partial T}{\partial r} + \frac{\partial^2 T}{\partial z^2}\right) \tag{2}$$

where r and z are the radial and axial coordinates respectively. In order to be used in REXCO-H code a finite difference form of Eq. (2) must be formulated. This is done by using the so-called mid-point method. The mid-point method was used to derive the finite difference equations for the hydrodynamic equations. The nomenclature defined in Fig. 1 will be used in the derivation of the difference form of Eq. (2). The derivation follows.

Expanding the temperature around point 0 in a Taylor Series one gets the following expressions for temperature at points 5, 6, 7 and 8:

$$T_5 = T_0 + (z_5 - z_0)\frac{\partial T}{\partial z} + (r_5 - r_0)\frac{\partial T}{\partial r} + \frac{(r_5 - r_0)^2}{2}\frac{\partial^2 T}{\partial r^2} + \frac{(z_5 - z_0)^2}{2}\frac{\partial^2 T}{\partial z^2} +$$

$$\frac{(z_5 - z_0)(r_5 - r_0)}{2} \frac{\partial^2 T}{\partial r \partial z} + \ldots \tag{3}$$

$$T_6 = T_0 + (z_6 - z_0) \frac{\partial T}{\partial z} + (r_6 - r_0) \frac{\partial T}{\partial r} + \frac{(r_6 - r_0)^2}{2} \frac{\partial^2 T}{\partial r^2} + \frac{(z_6 - z_0)^2}{2} \frac{\partial^2 T}{\partial z^2} +$$

$$\frac{(z_6 - z_0)(r_6 - r_0)}{2} \frac{\partial^2 T}{\partial r \partial z} + \ldots \tag{4}$$

$$T_7 = T_0 + (z_7 - z_0) \frac{\partial T}{\partial z} + (r_7 - r_0) \frac{\partial T}{\partial r} + \frac{(r_7 - r_0)^2}{2} \frac{\partial^2 T}{\partial r^2} + \frac{(z_7 - z_0)^2}{2} \frac{\partial^2 T}{\partial z^2} +$$

$$\frac{(z_7 - z_0)(r_7 - r_0)}{2} \frac{\partial^2 T}{\partial r \partial z} + \ldots \tag{5}$$

$$T_8 = T_0 + (z_8 - z_0) \frac{\partial T}{\partial z} + (r_8 - r_0) \frac{\partial T}{\partial r} + \frac{(z_8 - z_0)^2}{2} \frac{\partial^2 T}{\partial z^2} + \frac{(r_8 - r_0)^2}{2} \frac{\partial^2 T}{\partial r^2} +$$

$$\frac{(z_8 - z_0)(r_8 - r_0)}{2} \frac{\partial^2 T}{\partial z \partial r} + \ldots \tag{6}$$

Neglecting higher order terms, and subtracting Eq. (6) from Eq. (4) and Eq. (5) from Eq. (3) one gets

$$T_6 - T_8 = (z_6 - z_8) \frac{\partial T}{\partial z} + (r_6 - r_8) \frac{\partial T}{\partial r} \tag{7}$$

$$T_5 - T_7 = (z_5 - z_7) \frac{\partial T}{\partial z} + (r_5 - r_7) \frac{\partial T}{\partial r} \tag{8}$$

Then solving Eqs. (7) and (8) for the partials

$$\frac{\partial T}{\partial r} = - \frac{[(T_5 - T_7)(z_6 - z_8) - (T_6 - T_8)(z_5 - z_7)]}{(r_6 - r_8)(z_5 - z_7) - (r_5 - r_7)(z_6 - z_8)} \tag{9}$$

$$\frac{\partial T}{\partial z} = - \frac{(T_5 - T_7)(r_6 - r_8) - (T_6 - T_8)(r_5 - r_7)}{(r_6 - r_8)(z_5 - z_7) - (r_5 - r_7)(z_6 - z_8)} \tag{10}$$

The above equations for the evaluation of the first partials are now in terms of the temperatures and coordinates at points 5, 6, 7, and 8. However, in the Lagrangian code REXCO-H the specific internal energies and coordinates are known only at the center of each cell and at each mesh point respectively. To convert the above to temperatures at points 1, 2, 3 and 4 and coordinates at points A, B, C and D the following approximations are made since each mesh point is considered to be connected by a straight line.

$$T_5 = \frac{1}{2}(T_1 + T_2),\ T_6 = \frac{1}{2}(T_2 + T_3),\ T_7 = \frac{1}{2}(T_3 + T_4),$$

$$T_8 = \frac{1}{2}(T_1 + T_4),\ r_5 = \frac{1}{2}(r_A + r_0),\ r_6 = \frac{1}{2}(r_B + r_0),$$

$$r_7 = \frac{1}{2}(r_C + r_0),\ r_8 = \frac{1}{2}(r_D + r_0),\ z_5 = \frac{1}{2}(z_A + z_0),$$

$$z_6 = \frac{1}{2}(z_B + z_0),\ z_7 = \frac{1}{2}(z_C + z_0),\ z_8 = \frac{1}{2}(z_D + z_0) \tag{11}$$

Substituting Eq. (11) into Eqs. (9) and (10) and noting that

$$2A_1 = (r_6 - r_8)(z_5 - z_7) - (r_5 - r_7)(z_6 - z_8) \tag{12}$$

one then can find expressions for the first partials at point 0, in the form

$$\left(\frac{\partial T}{\partial r}\right)_0 = -\frac{1}{8A_1}\left[(T_1 - T_3)(z_A + z_B - z_C - z_D) - (T_2 - T_4)(z_A - z_B + z_D - z_C)\right] \tag{13}$$

$$\left(\frac{\partial T}{\partial z}\right)_0 = \frac{1}{8A_1}\left[(T_1 - T_3)(r_B - r_D + r_A - r_C) - (T_2 - T_4)(r_A - r_B - r_C + r_D)\right] \tag{14}$$

These equations can be generalized for any point (I,J) by making the appropriate substitutions as suggested in Fig. (1). Thus Eqs. (13) and (14) become

$$\left(\frac{\partial T}{\partial r}\right)_{I,J} = -\frac{1}{8A_{I,J}}\left[(T_{I,J} - T_{I-1,J-1})(z_{I,J+1} + z_{I-1,J} - z_{I,J-1} - z_{I+1,J}) - (T_{I-1,J} - T_{I,J-1})(z_{I,J+1} - z_{I-1,J} - z_{I,J-1} + z_{I+1,J})\right] \tag{15}$$

$$\left(\frac{\partial T}{\partial z}\right)_{I,J} = \frac{1}{8A_{I,J}}\left[(T_{I,J} - T_{I-1,J-1})(r_{I,J+1} + r_{I-1,J} - r_{I,J-1} - r_{I+1,J}) - (T_{I-1,J} - T_{I,J-1})(r_{I,J+1} - r_{I-1,J} - r_{I,J-1} + r_{I+1,J})\right] \tag{16}$$

where

$$A_{I,J} = -A_1 = \frac{1}{8}\left[(r_{I,J+1} - r_{I,J-1})(z_{I+1,J} - z_{I-1,J}) - (z_{I,J+1} - z_{I,J-1})(r_{I+1,J} - r_{I-1,J})\right] \tag{17}$$

The second term on the rhs of Eq. (2) may then be approximated by using the centroidal distance of the cell and the average first partial of the four corners of the cell, i.e.

$$\left(\frac{1}{R}\frac{\partial T}{\partial r}\right)_{I,J} = \frac{1}{R_{CENT}}\frac{\left(\frac{\partial T}{\partial r}\right)_{I,J} + \left(\frac{\partial T}{\partial r}\right)_{I+1,J} + \left(\frac{\partial T}{\partial r}\right)_{I+1,J+1} + \left(\frac{\partial T}{\partial r}\right)_{I,J+1}}{4} \tag{18}$$

where

$$R_{CENT} = \frac{r_{I,J} + r_{I+1,J} + r_{I+1,J+1} + r_{I,J+1}}{4}$$

The second partials can now be approximated in a similar manner where the mid-point method is applied a second time in which the first partial of the temperature is used in place of the temperature field. Thus

$$\left(\frac{\partial^2 T}{\partial r^2}\right)_{I,J} = \frac{1}{2A_{I,J}}\left\{\left[\left(\frac{\partial T}{\partial r}\right)_{I,J+1} - \left(\frac{\partial T}{\partial r}\right)_{I+1,J}\right](z_{I+1,\,J+1} - z_{I,J}) - \left[\left(\frac{\partial T}{\partial r}\right)_{I+1,J+1} - \left(\frac{\partial T}{\partial r}\right)_{I,J}\right](z_{I,J+1} - z_{I+1,J})\right\} \tag{19}$$

where

$$A_{I,J} = \tfrac{1}{2}\left[(z_{I+1,J+1} - z_{I,J})(r_{I+1,J} - r_{I,J+1}) - (r_{I+1,J+1} - r_{I,J})(z_{I+1,J} - z_{I,J+1})\right].$$

and

$$\left(\frac{\partial^2 T}{\partial z^2}\right)_{I,J} = \frac{-1}{2A_{I,J}}\left\{\left[\left(\frac{\partial T}{\partial z}\right)_{I,J} - \left(\frac{\partial T}{\partial z}\right)_{I+1,J+1}\right](r_{I+1,J} - r_{I,J+1}) - \left[\left(\frac{\partial T}{\partial z}\right)_{I,J+1} - \left(\frac{\partial T}{\partial z}\right)_{I+1,J}\right](r_{I+1,J+1} - r_{I,J})\right\} \tag{20}$$

Now we have a set of difference equations, compatible with the REXCO-H Lagrangian coordinate system, to solve the intercell conduction problem. This method of calculation, however has its drawbacks in that for sufficiently long times with relatively large time steps the solution diverges. This is demonstrated in the following example in which a comparison is made with an analytical and a numerical solution using a standard heat transfer code.

When developing a code one must be aware of its limitations. In this case, in order to develop a heat transfer code which is compatible with the Lagrangian system and which will not occupy too great a space in the program, the "normal" way of numerically solving the conduction equation is not used. By "normal" method of solution of the conduction equation in cylindrical coordinates is meant the following. For a transient solution of the conduction equation in cylindrical coordinates an equation is written for each individual point and the set of equations is solved simultaneously for each time step. Using this technique, however, the set of equations is not solved simultaneously but is solved point by point in one sweep each time step. For very short time steps this method is not too bad providing of course that the total number of time steps is not excessively high.

A test problem was run using the Lagrangian coordinate procedure outlined above. The problem delineated was that of an infinitely long solid steel rod 1 cm in radius, with a uniform temperature distribution of 1000°C, while the rod wall was assumed to be held at a temperature of 0°C. The following data were assumed for the steel:

$$k = 14.25 \frac{\text{Btu}}{\text{hr-ft-°F}} = 0.2465 \frac{\text{J}}{\text{sec-cm-°C}}$$

$$c = 0.1425 \frac{\text{Btu}}{\text{lb}_m\text{-°F}} = 0.596 \frac{\text{J}}{\text{gm-°C}}$$

$$\rho = 480 \frac{\text{lb}}{\text{ft}^3} = 7.7 \frac{\text{gm}}{\text{cm}^3}$$

$$\alpha = 0.053713 \frac{\text{cm}^2}{\text{sec}}$$

An analytical solution for this particular problem was derived. To establish the range of validity, or more properly, how well the mathematical model solves the actual problem several parameters were investigated. Among these were time step size and mesh size in the zone immediately outside the boundary, i.e., the zone which is held at 0°C throughout the solution. It was found that a better description of the temperature variation in the region of the boundary is improved if smaller zone sizes are used. However, in REXCO-H, it is desirable to have as uniform a grid spacing as possible to eliminate possible errors in calculation and to avoid the excessive computing time which may be needed due to the reduced grid size and time step.

Another parameter investigated was the effect of the time step on the solution. Due to the nature of the REXCO-H solution method, is that each time step is calculated by a sweep over the entire grid, it was necessary to understand how well the approximation approached the analytical heat conduction solution. To do this the time step was varied and the transient temperature distribution was compared to that obtained using the analytical solutions. It was found that for a typical time step of 10^{-5} sec a very good approximation to the true temperature distribution could be obtained for real times approaching 200 msec, or about an order of magnitude longer in time than REXCO-H calculation made to date for typical fast reactor configurations. However, some configurations involving low energy excursions may be extended, with rezoning, to times approaching 200 msec. The results of the comparison are shown in Fig. 2.

A small sample problem was run using the REXCO-H code with the heat conduction model included. The model chosen was essentially one dimensional in the radial direction and is shown in Fig. 3. Figure 3a shows the actual configuration while Fig. 3b depicts its representation in the Lagrangian mesh. The initial temperatures and pressures for each material are given. The calculation was performed with heat conduction and without heat conduction in order to compare results and determine the effect of conduction heat transfer both at the contact surface between the materials and that due to the shock wave. The differences, if any, would exist in the energy of each zone. Comparison of the results for a run up to 2000 cycles, or 7.82 msec, show the effect to be slight as expected. Table I lists various zones and their specific internal energy at 7.82 msec. It can be seen that at this time the charge is very slight, the effect appearing only in the sixth or seventh significant figure. However, it can be expected to become more significant as the time is extended or various thermal conductivities are used. This example used a thermal conductivity of $.303 \times 10^6$ for UO_2 gas and $.505 \times 10^7$ for liquid sodium. It is apparent that most of the energy increase in the sodium zones is due to compression of the gas since the pressure increases from 1 bar to about 300 kbar during the process. It should be noted that the pressure distribution is nearly constant at 2000 cycles throughout the system with much reduced pressure gradients.

The models' usefulness could be extended by prescribing various quantities for the thermal conductivity that would reflect more realistically heat transfer between fluids. As yet this has not been tried since it would be necessary to have sufficient data on which to base a modified thermal conductivity for a specific material or combination of materials.

5. FUEL-COOLANT INTERACTIONS AS AN ENERGY SOURCE

A further concern of reactor safety analysts is the possibility of excessively high pressure generation due to a molten fuel coolant interactions (MFCI). The possibility of a MFCI exists in a wide spectrum of accidents but is of most concern in accidents of fairly low energy where fuel is melted and can easily come into contact with sodium coolant. The possibility of a rapid energy transfer from fuel to sodium can cause high pressures due first to liquid sodium expansion followed by rapid sodium vapor generation and expulsion. For very rigid boundaries the liquid expansion phase may produce quite high pressures which could cause damage locally to subassemblies and perhaps propagate to other reactor structures. In order to take this phenomenon into account, especially for low energy whole core accidents as well as to study the phenomenon in smaller configurations such as single subassemblies, a fuel-coolant interaction capability has been built into REXCO-H. The heat transfer model itself is quite flexible and easily changed since it exists as a separate subroutine with REXCO. The main difficulty with providing this capability has been one of programming and the development of an equation of state for sodium which would allow the existence of liquid, liquid-vapor and vapor states to exist within a complex pressure field. No attempt has been made in this study to devise unique heat transfer models to describe fuel-coolant interactions. Only those already in existence were used.

The initial model used was that of the quasi-steady state heat transfer model devised by Cho and Wright [2]. The model is quite simple and was used since it was the easiest to incorporate and compare with existing results. One considers that a given amount of molten fuel with a given particle size has been dispersed in a zone of liquid sodium. The heat transfer is assumed to follow the convective relationship

$$\dot{q} = (hA)(T_f - T) \tag{21}$$

where $\dot{q}$ is the heat transfer rate, T_f is the fuel temperature, T is the sodium temperature and (hA) is a parametric convective heat transfer coefficient based on the fuel thermal conductivity and the particle size in which

$$h = \frac{k_f}{r_f}$$

and

$$A = 4\pi r_f^2$$

where k_f is the fuel thermal conductivity and r_f is the molten fuel particle radius. The model assumes that the main hindrance to heat transfer is the thermal conductivity of the fuel and that all heat entering the coolant in the interaction zone is dispersed uniformly and the sodium is in thermodynamic equilibrium throughout the process. The model is claimed to roughly account for a finite rate of fuel fragmentation.

Once a heat transfer model has been developed, a suitable equation of state for the sodium coolant should be devised to describe the three phases which the process passes through. This is shown in Fig. 4, a p-v curve of the process of fluid expansion first as a liquid then as a pure vapor. Initial heating of the liquid causes an essentially constant volume pressurization of the liquid as it is rapidly heated from a to b. The liquid expands slightly with corresponding pressure drop from b to c where the saturation pressure is reached. From c to d heat is still being added, if no heat transfer cut off is assumed due to vapor blanketing, while the mixture vaporizes with increasing pressure due to the constraints on the interaction zone. Finally at point d the sodium is completely vaporized and expands as a vapor. So to describe this process, a set of thermodynamic relationships are needed, i.e., an equation of state for sodium.

To calculate the effect of the thermal expansion of a liquid an equation of state based on the work of Anderson [3] was developed. Since the specific volume is a function of temperature and pressure one can write

$$dv = -\beta v dp + \alpha v dT \tag{22}$$

where v is the specific volume, β is the isothermal compressibility, p is the pressure, α is the coefficient of volume expansion and T is the temperature. Using Anderson's form for the isothermal compressibility

$$\beta = \frac{1}{B_o + B_o' p} = \frac{1}{B}$$

where

$B_o = B_{p \to o}$

B = isothermal bulk modulus

$B_o' = \left\{ \left(\frac{\partial B}{\partial p} \right)_T \right\}_{p \to o} = (B')_{p \to o}$.

Then, substituting the above into Eq. (22) and integrating we obtain

$$p = \frac{B_o}{B_o'}\left\{\left(\frac{v_o}{v}\right)^{B_o'} \exp\left[B_o' \int_{T_o}^{T} \alpha(T)dT\right] - 1\right\} \tag{23}$$

where v_o and T_o are the initial specific volume and temperature, v and T are the present values, and $\alpha(T)$ is the temperature dependent volumetric coefficient of thermal expansion. If $\alpha = 0$, then Eq. (23) reduces to Murnaghan's equation of state.

Treatment of the two phase state of sodium involves the specification of saturated liquid and vapor enthalpies and specific volumes plus the saturation pressure. The equations used in this model were adopted by Cho, Ivins and Wright [4] from the data of Golden and Tokar [5] and are as follows:

$$h_g = 0.7781 \times 10^{11} - 6.14965 \times 10^{7}T + 0.43455 \times 10^{5}T^2 - 9.7274T^3 \tag{24}$$

$$h_f = -3.8566 \times 10^{10} + 8.13507 \times 10^{7}T - 0.4399 \times 10^{5}T^2 + 9.3842T^3 \tag{25}$$

$$p_{sat} = 1.01325 \times 10^{6}T^{-.61344} \exp\left(15.3838 - \frac{12767.8}{T}\right) \tag{26}$$

$$v_g = 3.6132 \times 10^{6} \cdot \frac{zT}{p_{sat}} \tag{27}$$

$$v_f = v_{fo} \exp\left[\int_{T_o}^{T} \alpha(T)dT\right] \tag{28}$$

$$z = -0.97258 + 0.42417 \times 10^{-2}T - 0.28996 \times 10^{-5}T^2 + 0.55424 \times 10^{-9}T^3 \tag{29}$$

$$\alpha = 0.21968 \times 10^{-3} + 0.81226 \times 10^{-7}T + 0.97135 \times 10^{-11}T^2 + 0.68998 \times 10^{-15}T^3 \tag{30}$$

where T is the temperature in °K, h_g and h_f are the saturated vapor and liquid enthalpies in $\frac{\text{dyne-cm}}{\text{gm}}$, v_g and v_f are the saturated vapor and liquid specific volumes in $\frac{\text{cm}^3}{\text{gm}}$, z is the compressibility factor, p_{sat} is the saturation pressure in dyne/cm^2 and α is the volumetric coefficient of thermal expansion in °K^{-1}. The specific volume and enthalpy of a two phase mixture is given as

$$v = xv_g + (1 - x)v_f \tag{31}$$

$$h = xh_g + (1 - x)h_f \tag{32}$$

where x is the quality of the mixture. The known quantities for a given cell in REXCO-H are the specific volume and the specific internal energy from which the enthalpy is easily calculated. The unknown quantities are the temperature and quality of the mixture. To solve the set of Eqs. (31) and (32) using relations (24) to (30), a Newton-Raphson technique for a set of two, non-linear algebraic equations was applied. The technique is outlined briefly in the following:

Given two simultaneous non-linear equations of the form

$$\begin{aligned} F(x,T) &= 0 \\ G(x,T) &= 0 \end{aligned} \tag{33}$$

an initial guess at the solution is (x_o, T_o). However, the true solution is $(x_o + \delta_o, T_o + \varepsilon_o)$ so that

$$F(x_o + \delta_o, T_o + \varepsilon_o) = 0$$

and (34)

$$G(x_o + \delta_o, T_o + \varepsilon_o) = 0$$

Expanding Eq. (34) about (x_o,T_o) and neglecting higher order terms one gets

$$F(x_o,T_o) + \delta_o \left(\frac{\partial F}{\partial x}\right)_o + \varepsilon_o \left(\frac{\partial F}{\partial T}\right)_o = 0$$
$$G(x_o,T_o) + \delta_o \left(\frac{\partial G}{\partial x}\right)_o + \varepsilon_o \left(\frac{\partial G}{\partial T}\right)_o = 0 \quad (35)$$

Solving Eq. (35) for δ_o and ε_o, one then gets

$$\delta_o = \frac{-G(x_o,T_o)\left(\frac{\partial F}{\partial T}\right)_o + F(x_o,T_o)\left(\frac{\partial G}{\partial T}\right)_o}{\left(\frac{\partial G}{\partial T}\right)_o\left(\frac{\partial F}{\partial x}\right)_o - \left(\frac{\partial G}{\partial x}\right)_o\left(\frac{\partial F}{\partial T}\right)_o} \quad (36)$$

Then a second guess

$$(x_1,T_1) = (x_o + \delta_o, T_o + \varepsilon_o)$$

can be made and the process repeated until a suitable error criterion for (x,T) has been reached.

For the present case we have

$$F(x,T) = v - xv_g - (1 - x)v_f = 0$$

and

$$G(x,T) = h - xh_g - (1 - x)h_f = 0$$

where the quantities v_g, v_f, h_g, and h_f were defined earlier. It is straightforward to calculate the quantities $\left(\frac{\partial F}{\partial x}\right)_g$, $\left(\frac{\partial F}{\partial T}\right)$, $\left(\frac{\partial G}{\partial x}\right)$ and $\left(\frac{\partial G}{\partial T}\right)$ and solve for successive values of δ and ε until a suitable solution for the quality and temperature of the mixture (x,T) is reached based only on the specific volume and enthalpy. To solve for the pressure in the pure vapor phase Eq. (27) is used.

The above set of equations and the Newton-Raphson technique has been programmed for use in REXCO-H to permit the calculation of a wide spectrum of reactor safety problems ranging from single subassembly effects to those involving a whole reactor system up to the primary containment boundaries. It is hoped that in this way more proper treatment of lower energy excursions may be obtained as well as to extend the capability of the program into the molten core accident. Also, an added benefit of including both a subroutine to handle heat transfer on an intracell basis plus a two phase equation of state for sodium may permit the evaluation of plug jump problems in which energy is transferred from the hot, condensable, sodium vapor bubble to the cold structure existing above the core.

An example problem was defined to test the molten fuel-coolant interaction model and to obtain some preliminary insights into the coupling of hydrodynamic and structural effects. The model is shown in Fig. 5. The molten fuel-coolant interaction zone was considered to be 6 cm in radius and 30 cm long. Above this zone is a column of sodium 60 cm high topped by a 18 cm high section filled with argon at atmospheric pressure. The boundaries of the system were the variables studied in this example. The first case run considered the vessel wall to be rigid. The second considered the annulus outside the wall to be filled with sodium

while the third had argon gas in the annulus.

Initially the entire system was assumed to be at atmospheric pressure with the sodium at 1100°K and the molten fuel at 2900°K. The fuel particle diameter was assumed to be .0234 cm, while the volume fraction of sodium in each cell was assumed to be .568 and the volume fraction of UO_2 was assumed to be 0.432. The densities of sodium and UO_2 were 0.7568 and 9.0 g/cm^3 respectively, and the sodium to fuel weight ratio was 0.1106 or the ratio which will usually give a maximum amount of destructive work for a given molten fuel-coolant interaction.

As mentioned above, three cases were run using the model shown in Fig. 6, in order to get some preliminary knowledge of the behavior of a molten fuel-coolant interaction coupled to compressible hydrodynamics and structural deformations. The first case run was that of a rigid wall. The pressure-time history at the center of the interaction zone (cell 2,4) is shown in Fig. 7. This represents a non-classic shape in which the pressure peak is due to the rapid heating of the sodium coolant at an almost constant volume. At approximately .6 msec the pressure falls to the local saturation pressure and vaporization begins. The pressure increases to the completion of the problem due to the increase of the local saturation pressure. This problem represents the simplest, one-dimensional case and has essentially been solved by the use of ordinary differential equations, and is generally well behaved. This coupling with the hydrodynamic code REXCO-H, however, eliminates the need to differentiate between acoustic and inertial constraints [4]. The maximum pressure developed in this case was 1.29×10^9 dyne/cm^2 or 19.1×10^3 psi. At the termination of the problem at 28 msec the upper surface had moved about 17 cm. Thus in this case, all the work potential generated in the fuel-coolant interaction was divided between the compressive energy stored in all the fluids; kinetic energy of the fluids and the heat stored in the sodium in the fuel-coolant interaction zone.

Case two involved an MFCI zone bounded on the top by 60 cm of sodium and on the side by an elastic steel wall 0.254 cm thick. This was surrounded by a 6 cm thick annulus of sodium and the entire system was bounded by a rigid wall. Thus the maximum radial displacement of the steel wall was 6 cm. The pressure time history in the center of the MFCI zone is shown in Fig. 8. Here the effect of the wall is quite clearly seen in two ways. First the maximum pressure in the liquid expansion phase is down to about 3.40×10^8 dynes/cm^2 (5033 psi) or about one fourth of the peak value in the rigid wall case. Vaporization begins at approximately the same time at 0.6 msec. Inclusion of the wall, however, shows quite complex pressure time history in which pressure peaks are superimposed on the liquid and vapor expansion phases. Although no absolute reasons can be given for these peaks, it does seem possible that they are related to the natural frequency of the system. The period of a ring with the same dimensions as the vessel is 0.074 sec while the period is actually about 0.15 sec. This difference may be due to the mass of the sodium inside and outside the vessel. It can also be seen that the period increases with time and may be related to vaporization effects.

The third case was similar to that of case two except that argon gas was placed in the annulus around the steel vessel. The pressure-time plot is shown in Fig. 9. Again the pressure peaks appear and are of about the same frequency as the previous case. Since no resistance is given by the argon gas annulus the pressure is reduced to 2.5×10^8 dyne/cm^2 (3700 psi) and vaporization starts at about 0.3 msec, a factor of two faster than cases one and two. The following pressure peaks, however, cause recondensation and the zone ultimately

partially vaporizes and recondenses. The most interesting part of these preliminary calculations, is that due to wall movement on the boundary of the MFCI zone the possibility of reduced peak liquid pressures exist plus the fact that since vaporization may occur faster, vapor blanketing of the fuel particles may well reduce the amount of heat transferred from fuel to sodium.

6. CONCLUSION

Although heat transfer problems in post burst accident analyses in LMFBR is at present somewhat nebulous and not easily given to a general treatment, models can be developed to accommodate specific cases. A calculational model to handle heat conduction between cells has been developed and included in the hydrodynamic code REXCO-H. Although the effect is negligible, as expected, it does point the way to consideration of intercell heat transfer by using appropriate, modified thermal conductivities.

A specific model to consider molten-fuel-coolant interactions has been used. Here the coupling of the MFCI model with a more realistic set of hydrodynamic equations with structural considerations allows one to more accurately assess the destructive potential of such events on the reactor structure. Based on preliminary results, the possibility exists for early heat transfer cut off due to sodium vapor formation.

ACKNOWLEDGMENTS

A note of thanks are due to Drs. S. H. Fistedis and Y. W. Chang for fruitful discussion concerning containment problems in general and heat transfer problems in particular and to Messrs. J. Gvildys and R. Julke who not only helped me to understand somewhat the intricacies of REXCO-H, but also to change the program to suit the needs of the present study. Thanks are also due to Dr. D. H. Cho for his aid in providing the initial fuel-coolant interaction models and sodium equation of state.

REFERENCES

[1] Chang, Y. W., Gvildys, J. and Fistedis, S. H., "Two-Dimensional Hydrodynamics Analysis for Primary Containment," USAEC Report ANL-7498 (November 1969).

[2] Cho, D. H. and Wright, R. W., "A Rate-Limited Model of Molten Fuel-Coolant Interactions," Trans. Am. Nucl. Soc., 13, 2, pp. 658-659 (November 1970).

[3] Anderson, O. L., "The Use of Ultrasonic Measurements under Modest Pressure to Estimate Compression at High Pressure," J. Phys. Chem. Solids, Pergamon Press, 1966, 27, pp. 547-565.

[4] Cho, D. H., Ivins, R. O., and Wright, R. W., Private communication.

[5] Golden, G. H., and Tokar, J. V., "Thermophysical Properties of Sodium," USAEC Report ANL-7323 (August 1967).

Table 1. Comparison of Specific Internal Energies for Example with and without Heat Conduction at t = 7.82 msec

Zone		Energy (dyne-cm/g x 10^{10})		
R	Z	Without Heat Transfer	With Heat Transfer	at t = 0
2	3	1.978579	1.978580	2.2051
21	3	1.874072	1.874074	2.2051
22	3	1.273710	1.274133	.75764
33	3	1.205895	1.205895	.75764
41	3	1.221155	1.221133	.75764
42	3	.3494635	.3494656	.3459510

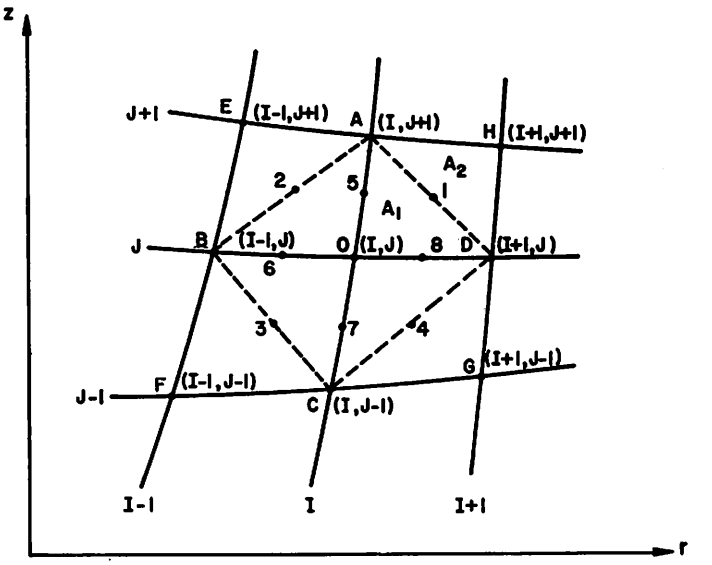

1. Nomenclature used in derivation of finite difference equation.

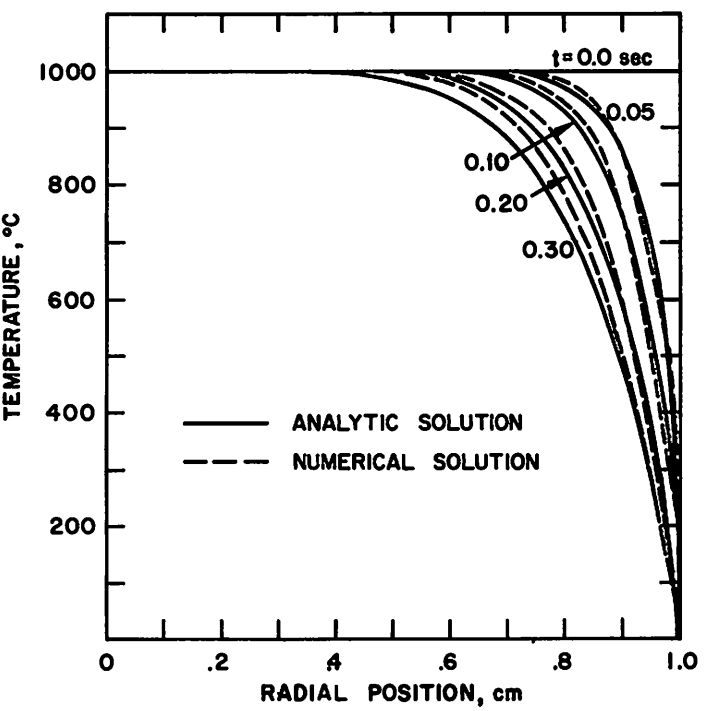

2. Comparison of heat conduction model to analytic solution.

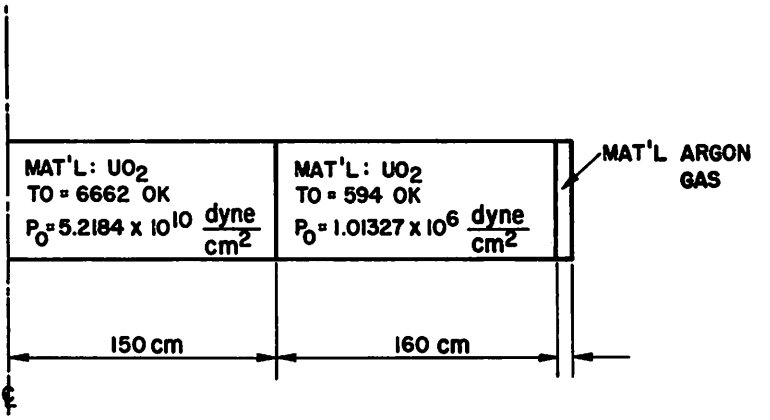

3a Schematic of heat conduction sample problem.

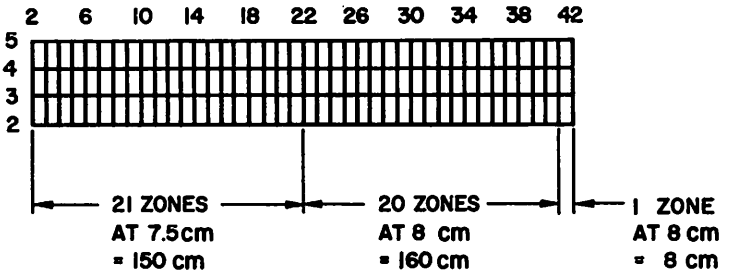

3b REXCO-H representation of sample problem.

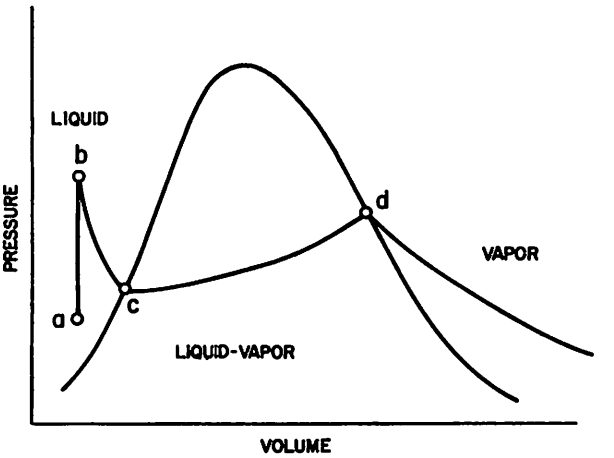

4. Volume expansion during fuel-coolant interaction.

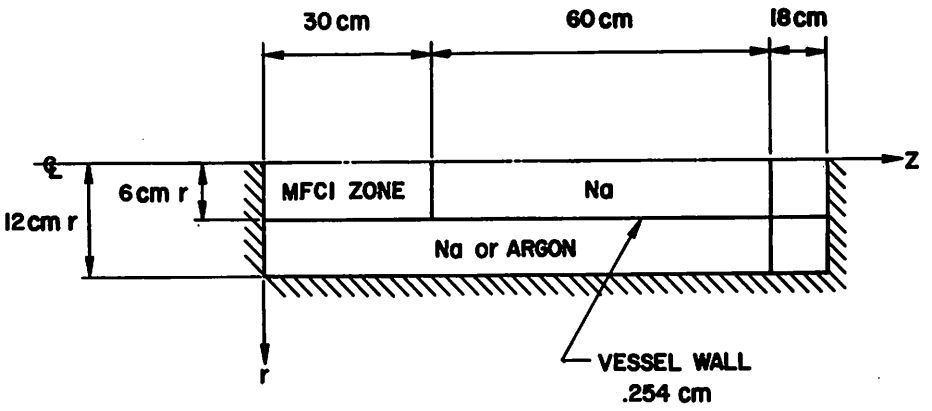

5. Fuel-coolant interaction test model.

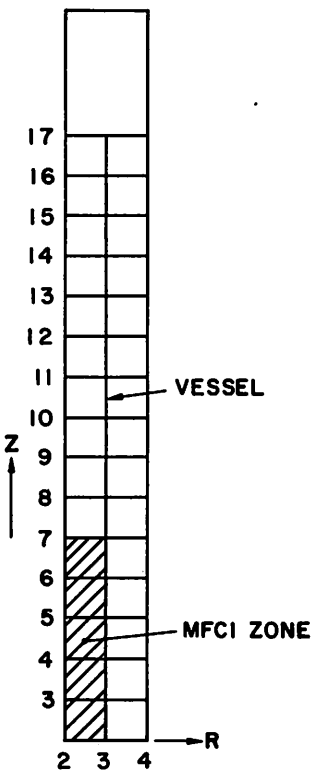

6. REXCO-H representation of MFCI example.

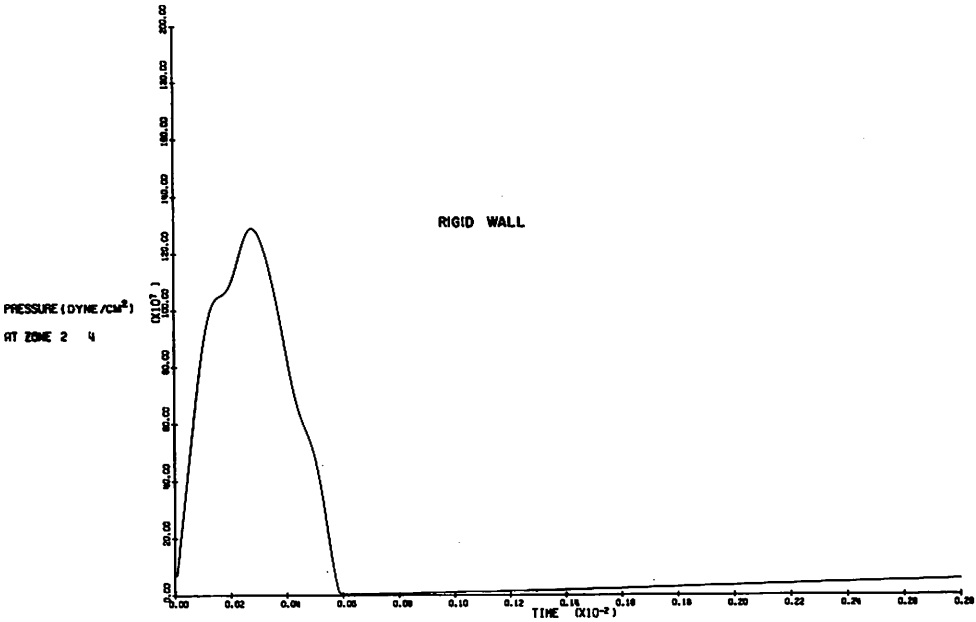

7. Pressure-time history at zone (2,4) for MFCI with rigid wall.

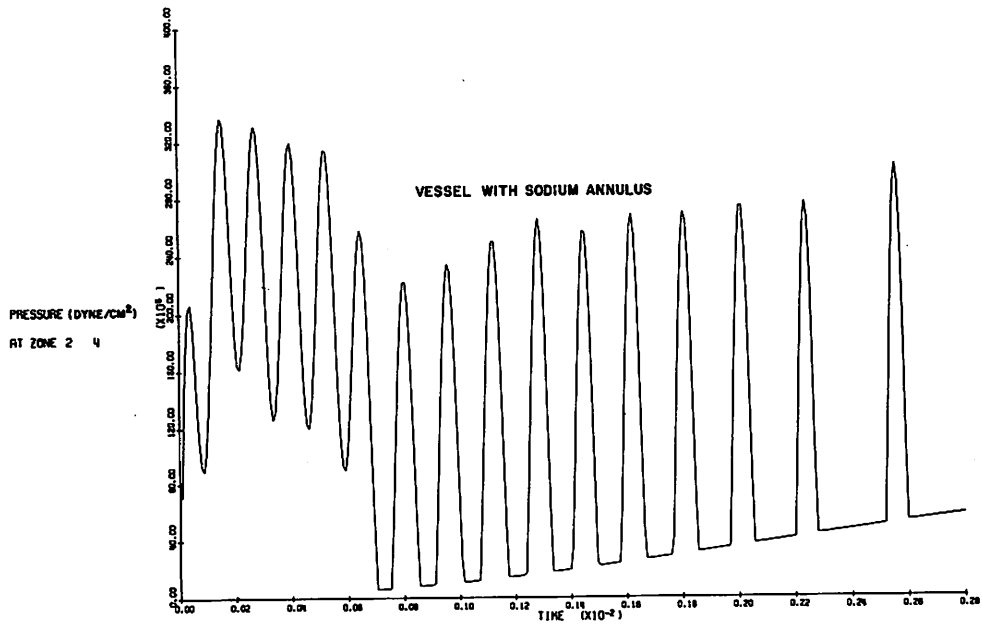

8. Pressure-time history at zone (2,4) for MFCI with vessel and sodium annulus.

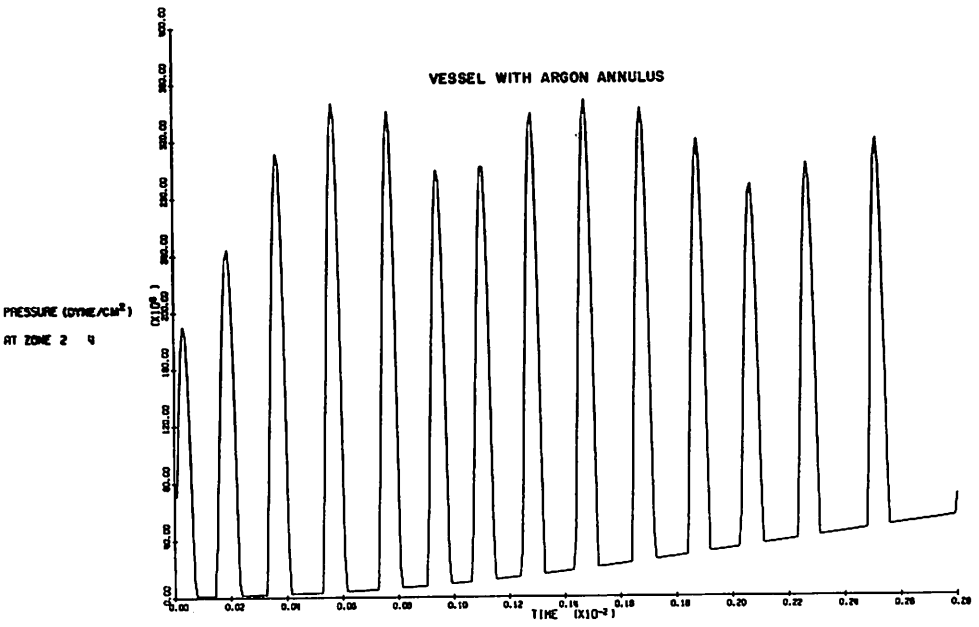

9. Pressure-time history at zone (2,4) for MFCI with vessel and argon annulus.